J Stat Phys (2017) 168:447–469
DOI 10.1007/s10955-017-1809-8

Power Spectrum of a Noisy System Close to a Heteroclinic Orbit

Jordi Giner-Baldó[1] · Peter J. Thomas[2] · Benjamin Lindner[1,3]

Received: 27 February 2017 / Accepted: 3 May 2017 / Published online: 16 May 2017
© Springer Science+Business Media New York 2017

Abstract We consider a two-dimensional dynamical system that possesses a heteroclinic orbit connecting four saddle points. This system is not able to show self-sustained oscillations on its own. If endowed with white Gaussian noise it displays stochastic oscillations, the frequency and quality factor of which are controlled by the noise intensity. This stochastic oscillation of a nonlinear system with noise is conveniently characterized by the power spectrum of suitable observables. In this paper we explore different analytical and semianalytical ways to compute such power spectra. Besides a number of explicit expressions for the power spectrum, we find scaling relations for the frequency, spectral width, and quality factor of the stochastic heteroclinic oscillator in the limit of weak noise. In particular, the quality factor shows a slow logarithmic increase with decreasing noise of the form $Q \sim [\ln(1/D)]^2$. Our results are compared to numerical simulations of the respective Langevin equations.

1 Introduction

Stochastic oscillations are a ubiquitous phenomenon in many fields of science. In biology, for instance, we see oscillatory behavior with a pronounced randomness in the concentration of intracellular calcium [11], in the mechanical motion of sensory organelles like the hair bundle [15], or in the concerted activity of nerve cells [2]. In physics such stochastic oscillations are the outcome of noisy laser dynamics [21] or of underdamped Brownian motion in a potential well. Other examples are the stochastic Brusselator model or the repressilator system from biochemistry [3].

✉ Benjamin Lindner
benjamin.lindner@physik.hu-berlin.de

1 Bernstein Center for Computational Neuroscience, Haus 2, Philippstr. 13, 10115 Berlin, Germany

2 Department of Mathematics, Applied Mathematics, and Statistics, Case Western Reserve University, Cleveland, OH 44106, USA

3 Department of Physics, Humboldt Universität zu Berlin, Newtonstr 15, 12489 Berlin, Germany

Whatever their physical origin, it is advantageous to describe stochastic oscillations in the Fourier domain, i.e. in terms of the power spectrum and its characteristics, such as peak frequency and line width. Simple linear systems, for instance, a harmonic oscillator with noise and damping, can often be employed as a model of stochastic oscillations. In this case, one can quickly determine the power spectrum by standard methods [5]. However, often we have to deal with self-sustained oscillations subject to noisy influences, i.e. inherently nonlinear systems driven by fluctuations. Moreover, there are systems, e.g. excitable systems, in which only a sufficient amount of (possibly random) external driving elicits a stochastic oscillation. Another example are heteroclinic systems [1,20,23], in which noise maintains an oscillation, and the intensity of the driving fluctuations controls the frequency and quality of the oscillation.

In nonlinear systems, the calculation of the key characteristics of noisy oscillations, the power spectrum, is a non-trivial task, for which no systematic method exists (for a number of exceptions, see [7,9,10,13]). Here, we present analytical and semianalytical results for a heteroclinic system, in which white Gaussian noise evokes stochastic oscillations. We are particularly interested in the weak-noise limit of the spectral statistics.

Our paper is organized as follows. In the next section, we introduce the stochastic model and the statistical measures of interest. We then show how we can extract the power spectrum from the Fokker–Planck equation associated with the model. After this, we consider the spectrum in the limit of weak noise and develop analytical approximations of varying complexity. We conclude with a short summary of our results.

2 Model and Measure of Interest

Heteroclinic cycling was first described in a three-population competitive interaction model by May and Leonard [16], and has been observed in models of neural systems exhibiting "winnerless competition" [19]. Suppose a system of differential equations possesses multiple isolated fixed points $\{\mathbf{p}_i\}_{i=1}^n$ of saddle type. If there is a sequence of heteroclinic trajectories $\{\gamma_i(t)\}_{i=1}^n$ starting and ending on the ith and $i+1$st saddle points, respectively (that is, $\lim_{t\to-\infty}\gamma_i(t) = \mathbf{p}_i$ and $\lim_{t\to\infty}\gamma_i(t) = \mathbf{p}_{i+1}$, identifying $n+1$ with 1), the union of the paths and their original/terminal points, Γ, forms a heteroclinic cycle. Assuming the unstable manifold of each point is one-dimensional, let $\lambda_{u,i} > 0$ be the unstable eigenvalue and $\lambda_{s,i}$ the stable eigenvalue with least negative real part for saddle point $\mathbf{p}_i$. If the product of the saddle values $\nu \equiv \Pi_{i=1}^n \left(-\Re\left[\lambda_{s,i}\right]/\lambda_{u,i}\right)$ is greater than unity, then the heteroclinic cycle is asymptotically stable, and there is a neighborhood around Γ within which trajectories converge towards Γ. Although the heteroclinic cycle may be structurally unstable, the neighborhood around it is robust to small perturbations, and is called a *heteroclinic channel* [18].

The system of interest here is a planar stochastic heteroclinic oscillator, first studied in [25] to test a new definition of phase of a stochastic oscillation (the noiseless, i.e. deterministic version of the model was introduced in [22]; *cf.* also Fig. 10.2 of [8]). It is given by the following two stochastic differential equations

$$\begin{aligned}\dot{y}_1 &= \cos(y_1)\sin(y_2) + \alpha\sin(2y_1) + \sqrt{2D}\xi_1(t),\\ \dot{y}_2 &= -\sin(y_1)\cos(y_2) + \alpha\sin(2y_2) + \sqrt{2D}\xi_2(t).\end{aligned} \tag{1}$$

We consider the dynamics on the domain $-\pi/2 \le \{y_1, y_2\} \le \pi/2$, impose reflecting boundary conditions, and restrict the parameter $\alpha \in (0, 1/2)$. For $D = 0$, the vector field has saddle

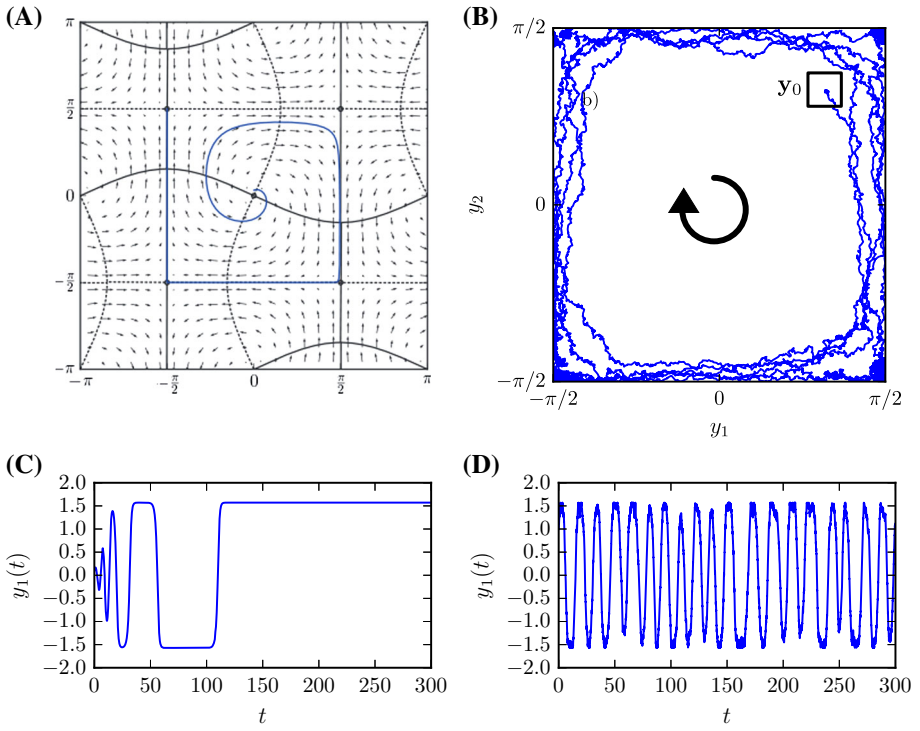

Fig. 1 Deterministic and stochastic versions of the heteroclinic system. **a** Phase portrait of the deterministic system with the trajectory shown in *blue*. The trajectory passes the four distinct saddle points (indicated by *thick black dots*), slowing down progressively as it gets closer to the stable heteroclinic cycle. Modified with permission from [22]. **b** The system with noise displays noisy clockwise rotations. **c** One of the components in the noiseless system exhibits a slowing down. **d** Endowed with white Gaussian noise, the same variable displays somewhat noisy but pronounced oscillatory behavior, resembling self-sustained oscillations which are perturbed by noise. Parameters: $\alpha = 0.1$ (all panels), $D = 0.01$ (**b**, **d**)

points at the four corners of the domain, each with eigenvalues $\lambda_u = 1 - 2\alpha$, $\lambda_s = -1 - 2\alpha$, and saddle values $\nu_i = (1 + 2\alpha)/(1 - 2\alpha) > 1$, for $i \in \{1, 2, 3, 4\}$. The white noise sources $\xi_{1,2}(t)$ are uncorrelated ($\langle \xi_i(t)\xi_j(t')\rangle = \delta(t - t')\delta_{i,j}$) and enter the equations multiplied by a factor that involves the noise intensity D.

In Fig. 1 we illustrate the emergence of pronounced oscillations that become apparent as noisy clockwise rotations in the (y_1, y_2) plane [cf. panel (B)] but can also be seen if a single variable is plotted vs time [cf. panel (D)]. Without noise, the dynamics goes from the neighborhood of one saddle to that of the next one [cf. panel (A)], slowing down while approaching in this way the heteroclinic orbit (which would have an infinite period). Consequently, oscillations in one of the variables have a transient nature [cf. panel (C)] and are not self-sustained.

Of course, if $y_1(t)$ oscillates, then so do observables that are functions of $y_1(t)$. In the following, we consider the observable

$$z_1(t) = \sin(y_1(t)). \tag{2}$$

In Fig. 2a, we show typical trajectories of the system's variable $y_1(t)$ and the observable $z_1(t)$. It will turn out that for $z_1(t)$ the determination of the power spectrum by Fokker–

Planck methods is particularly simple. Furthermore, for later analytical efforts, it will be helpful to consider the pair of transformed variables $[z_1 = \sin(y_1), z_2 = \sin(y_2)]$, that satisfy

$$\dot{z}_1 = (1 - z_1^2)(2\alpha z_1 + z_2) + \sqrt{2D(1 - z_1^2)}\xi_1(t),$$
$$\dot{z}_2 = (1 - z_2^2)(2\alpha z_2 - z_1) + \sqrt{2D(1 - z_2^2)}\xi_2(t). \tag{3}$$

In contrast to the original system, these stochastic differential equations include multiplicative noise terms, that must be interpreted in the sense of Stratonovich [5].

To characterize the oscillation of the system, we study the power spectrum of $z_1(t)$, defined in terms of the Fourier transform $\tilde{z}_1 = \int_0^T dt\, z_1(t)e^{2\pi i f t}$ or the autocorrelation function $C_{z1,z1}(\tau) = \langle z_1(t)z_1(t+\tau)\rangle$ by

$$S(f) = \lim_{T\to\infty} \frac{\langle \tilde{z}_1 \tilde{z}_1^* \rangle}{T} = \int_{-\infty}^{\infty} d\tau \langle z_1(t)z_1(t+\tau)\rangle e^{2\pi i f \tau}, \tag{4}$$

respectively. (Occasionally, we will refer also to the cyclic frequency $\omega = 2\pi f$.) The first definition can be easily applied to the trajectories resulting from numerical simulations (then, of course, only for a finite T), while the second relation is useful in our (semi)analytical calculations below. Numerically determined spectra of $y_1(t)$ and $z_1(t)$ are shown and compared in Fig. 2b. It becomes evident that at least the main peak at small frequencies (corresponding to the frequency of stochastic oscillations) is rather similar for $y_1(t)$ and $z_1(t)$. The main difference between these variables is the amplitude: while $y_1(t)$ varies between $-\pi/2$ and $\pi/2$, the variable $z_1(t)$ oscillates between ± 1. Consequently, if we plot the spectrum of $(\pi/2)z_1(t)$ (blue line in Fig. 2b), the spectrum is close to that of the original variable near the low-frequency peak.

The aim of our study is to provide results for the power spectrum and the characteristics of its main peak (frequency, peak width, and corresponding quality factor) as functions of the noise. We are especially interested in the weak-noise limit where these statistics should attain a simple and somewhat universal character that depends only on the fact that the system is close to the heteroclinic cycle.

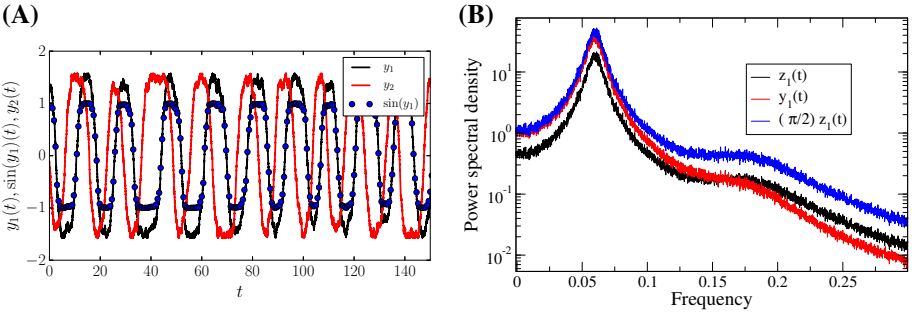

Fig. 2 **a** Time series of the system's variables $y_1(t)$ (*black*), $y_2(t)$ (*red*) and of the observable $z(t) = \sin(y_1(t))$ (*blue dots*). **b** Power spectra of $y_1(t)$ (*black*), $z(t)$ (*red*), and the rescaled variable $(\pi/2)z(t)$ (*blue*), which has the same maximal amplitude as $y_1(t)$. All spectra show a peak around $f = 0.06$ with similar height and width if the amplitudes are comparable (*red* and *blue lines*). Parameters: $D = 0.01$, $\alpha = 0.1$

3 Derivation of the Power Spectrum from the Fokker–Planck Equation

The approach to the calculation of the power spectrum of $z_1(t)$ presented in this section relies on the Fokker–Planck formalism [21] and it should be mentioned that similar techniques have been applied for a number of other nonlinear stochastic systems (see e.g. [7,10,14]).

The transition probability density $P(\mathbf{y}, \tau|\mathbf{y}', 0)$ of the stationary stochastic process $\mathbf{y}(t) = (y_1(t), y_2(t))$ satisfies the time-dependent Fokker–Planck equation

$$\partial_\tau P(\mathbf{y}, \tau|\mathbf{y}', 0) = \mathcal{L}_{\mathrm{FP}}(\mathbf{y}) P(\mathbf{y}, \tau|\mathbf{y}', 0), \tag{5}$$

with initial condition $P(\mathbf{y}, 0|\mathbf{y}', 0) = \delta(\mathbf{y} - \mathbf{y}') \equiv \delta(y_1 - y_1')\delta(y_2 - y_2')$. The Fokker–Planck operator $\mathcal{L}_{\mathrm{FP}}$ reads in this case

$$\begin{aligned}\mathcal{L}_{\mathrm{FP}} =& \frac{\partial}{\partial y_1}\left(-\cos(y_1)\sin(y_2) - \alpha\sin(2y_1) + D\frac{\partial}{\partial y_1}\right) \\ &+ \frac{\partial}{\partial y_2}\left(\sin(y_1)\cos(y_2) - \alpha\sin(2y_2) + D\frac{\partial}{\partial y_2}\right).\end{aligned} \tag{6}$$

Furthermore, the stationary probability density $P_0(\mathbf{y})$ satisfies the time-independent Fokker–Planck equation,

$$\partial_\tau P_0(\mathbf{y}) = 0 = \mathcal{L}_{\mathrm{FP}}(\mathbf{y}) P_0(\mathbf{y}). \tag{7}$$

For any nonlinear function $z(t) = f(\mathbf{y}(t))$, its autocorrelation function $C_{zz}(\tau) = \langle f(\mathbf{y}(0)) f(\mathbf{y}(\tau))\rangle - \langle f(\mathbf{y}(0))\rangle\langle f(\mathbf{y}(\tau))\rangle$ can be expressed by the following integral over the transition probability

$$C_{zz}(\tau) = \int d^2\mathbf{y}\, d^2\mathbf{y}'\, f(\mathbf{y}) f(\mathbf{y}') P_0(\mathbf{y}') \left[P(\mathbf{y}, \tau|\mathbf{y}', 0) - P_0(\mathbf{y})\right], \tag{8}$$

and thus we can write the power spectrum as

$$\begin{aligned}S_{zz}(\omega) &= 2\Re \int d^2\mathbf{y}\, d^2\mathbf{y}'\, f(\mathbf{y}) f(\mathbf{y}') P_0(\mathbf{y}') \int_0^{+\infty} d\tau\, e^{i\omega\tau} \left[P(\mathbf{y}, \tau|\mathbf{y}', 0) - P_0(\mathbf{y})\right], \\ &= 2\Re \int d^2\mathbf{y}\, f(y_1) \tilde{H}(\mathbf{y}; \omega).\end{aligned} \tag{9}$$

In the last line, we have introduced the auxiliary function

$$\tilde{H}(\mathbf{y}; \omega) = \int d^2\mathbf{y}'\, f(\mathbf{y}') P_0(\mathbf{y}') \int_0^{\infty} d\tau\, e^{i\omega\tau} \left[P(\mathbf{y}, \tau|\mathbf{y}', 0) - P_0(\mathbf{y})\right]. \tag{10}$$

By a number of straightforward manipulations (one-sided Fourier transformation of the Fokker–Planck Eq. 5, integration by parts, etc.; see [6]), we arrive at an equation for $\tilde{H}(\mathbf{y}; \omega)$:

$$\left(\mathcal{L}_{\mathrm{FP}}(\mathbf{y}) + i\omega\mathcal{I}\right) \tilde{H}(\mathbf{y}; \omega) = -P_0(\mathbf{y}) \left[f(\mathbf{y}) - \langle f(\mathbf{y})\rangle\right], \tag{11}$$

where $\mathcal{I}$ is the identity operator. The inhomogeneity in this partial (but time-independent) differential equation involves the steady-state probability density $P_0(\mathbf{y})$, which can be found from the stationary Fokker–Planck Eq. 7.

Solving the coupled system of partial differential equations, Eqs. 7 and 11, can be performed numerically by expanding the solutions in an appropriate basis of functions that satisfy the boundary conditions, and determining a sufficient number of the respective coefficients by solving the resulting system of linear equations, a technique that we refer to as the

matrix-inversion method in the following. We choose harmonic functions that automatically satisfy the periodic boundary conditions:

$$P_0(\mathbf{y}) = \sum_{m=-\infty}^{\infty} \sum_{l=-\infty}^{\infty} c_{m,l} e^{i(my_1 + ly_2)} \tag{12}$$

and

$$\tilde{H}(\mathbf{y};\omega) = \sum_{m=-\infty}^{\infty} \sum_{l=-\infty}^{\infty} \tilde{H}_{m,l}(\omega) e^{i(my_1 + ly_2)}. \tag{13}$$

For this choice, the power spectrum of the specific function $z(t) = z_1(t) = \sin(y_1)$ has the particularly simple form of a single coefficient

$$S_{z_1 z_1}(\omega) = (2\pi)^2 \Re\left[-i\left(\tilde{H}_{-1,0} - \tilde{H}_{0,1}\right)\right] = -8\pi^2 \Im\left[\tilde{H}_{0,1}(\omega)\right], \tag{14}$$

where $\Re$ and $\Im$ denote the real and imaginary parts, respectively, and we have used for the last equality that $\tilde{H}_{m,l} = -\tilde{H}_{-m,-l}$.

In order to determine the sets of coefficients $\{c_{m,l}\}$ and $\{\tilde{H}_{m,l}(\omega)\}$ we substitute the expansions Eqs. 12 and 13 into the differential equations Eqs. 7 and 11. In this way one obtains, for each of the two differential equations, a system of linear equations to which standard numerical matrix methods can be applied. This is a two-step process: we start by inserting the expansion for $P_0(\mathbf{y})$, Eq. 12, into Eq. 7, which yields a homogeneous system of linear equations for the coefficients $\{c_{m,l}\}$. This system has a unique solution if we add the normalization condition

$$\int_\Omega d\mathbf{y}\, P_0(\mathbf{y}) = 1, \quad \Omega = [-\pi/2, \pi/2] \times [-\pi/2, \pi/2]. \tag{15}$$

Once the coefficients $\{c_{m,l}\}$ are numerically determined they can be used to construct the RHS of Eq. 11, where we also substitute the expansion for $\tilde{H}(\mathbf{y};\omega)$, Eq. 13. By solving the resulting inhomogeneous system of linear equations on each point of a discretization $\{\omega_i\}, i = 1, \ldots, N$ of the interval $\omega \in (0, \omega_{max}]$ (containing the relevant part of the power spectrum) we obtain the set of coefficients $\{\tilde{H}_{m,l}(\omega_i)\}, i = 1, \ldots, N$ and hence the power spectrum. Appendix A provides details of the method, which was implemented in Python's programming language using the `numpy` library, and the methods for sparse matrices available in the `scipy.sparse.linalg` library.

In order to apply the numerical methods we first truncate the expansions Eqs. 12 and 13 at some $|m|, |l| = L$, so that the size of the matrix systems to be solved increases with L. At low noise levels, the distributions become more peaked, displaying abrupt changes on finer and finer spatial scales. Accurately describing this fine-scale structure requires the inclusion of modes $e^{imy_1} e^{ily_2}$ with higher spatial frequencies $|\mathbf{k}| = \sqrt{m^2 + l^2}$ in the expansion of $P_0(\mathbf{y})$ and $\tilde{H}(\mathbf{y};\omega)$. Representing these higher-resolution spatial scales is equivalent to increasing L, resulting in large matrices.

Figure 3 shows the resulting spectrum and corresponding simulation results for three noise levels, $D = 10^{-1}$ (red triangles), 10^{-2} (blue circles), and 10^{-3} (green squares). The figure illustrates the excellent agreement between Langevin simulations and the matrix-inversion method. As expected, the spectra show a strong primary peak that narrows and shifts towards lower frequencies for decreasing noise levels. Furthermore, for decreasing noise, the anharmonicity of the oscillation becomes more apparent, as secondary peaks at odd multiples of the fundamental frequency emerge (Fig. 3, black arrows).

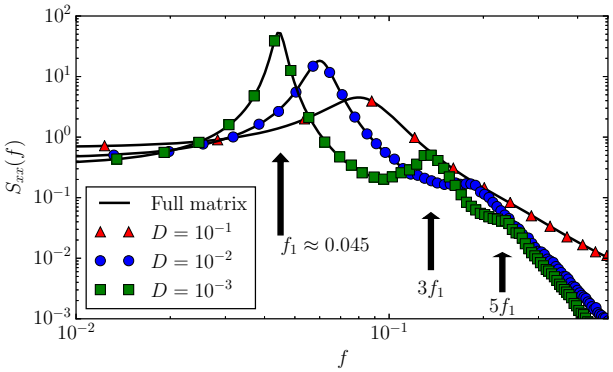

Fig. 3 Power spectrum of $\sin(y_1)$ for three noise levels. Results from stochastic simulations (*symbols*) agree with the matrix-inversion method (*black solid line*) for $D = 10^{-1}$ (*red*), 10^{-2} (*blue*), and 10^{-3} (*green*) over the frequency range shown. *Black arrows* indicate the frequency of the first peak and its higher (odd) harmonics for $D = 10^{-3}$. Parameters: $\alpha = 0.1$

For lower noise intensities, the size of the matrices required to accurately represent the system grows prohibitively, limiting application of the matrix-inversion method. Therefore, we explore in the next section an analytical approach to the weak-noise regime.

4 Weak-Noise Limit of the Power Spectrum

In this section we develop an analytical approach resulting in expressions for the power spectrum and for its characteristic features (the center frequency and width of the primary peak), valid for small noise levels. We introduce a sequence of three successively more refined approximations.

4.1 Two-State Process Approximation to the Primary Spectral Peak

First we consider an approximation valid at low frequencies, based on an alternating renewal process.

At low noise intensity, we observe that $z_1(t) = \sin(y_1(t))$ begins to resemble a dichotomous process (see Fig. 4), i.e. the variable remains close to one of two states ± 1 most of the time.

In the (y_1, y_2) plane, one cycle consists of passage through four corners. The probability distributions of passage times around single corners, $\{T_1, \ldots, T_4\}$, are governed by [23]

$$\rho_D(t) = \frac{2\lambda_u \Delta_D(t) e^{-\Delta_D^2(t)}}{\sqrt{\pi}(1 - e^{-2\lambda_u t}/(1 + \lambda_u/\lambda_s))} \tag{16}$$

where

$$\Delta_D(t) = \delta \left(\frac{2D}{\lambda_u} \left(e^{2\lambda_u t} \left(1 + \frac{\lambda_u}{\lambda_s} \right) - 1 \right) \right)^{-1/2}, \quad \lambda_u = 1 - 2\alpha, \lambda_s = 1 + 2\alpha. \tag{17}$$

In [23] the constant δ defines the size of a neighborhood around the heteroclinic saddle point for which the transit time distribution is obtained. The result is exact for a linear flow. For our nonlinear system we consider the transit time "around one corner" to be the time

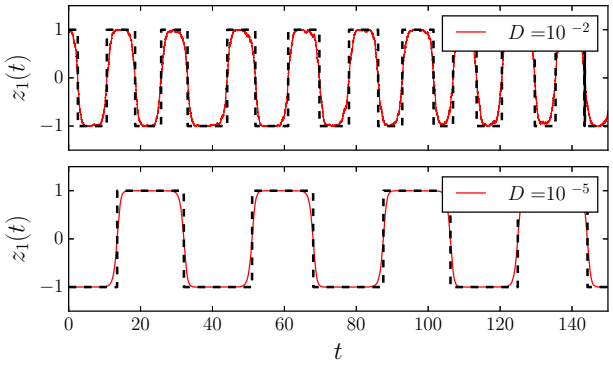

Fig. 4 Trajectory of the observable $z_1(t)$ for two values of the noise, $D = 10^{-2}$ (*upper panel*) and $D = 10^{-5}$ (*lower panel*). We show the approximation by a dichotomous noise, Eq. 21 (*dashed black line*) superimposed on a trajectory obtained from numerical simulations (*solid red line*)

required to pass through one quadrant of the domain. For small noise, and initial conditions close to the stable manifold of the saddle (the outer wall of the domain), the transit time is determined mainly by the portion of the trajectory in a small neighborhood surrounding the saddle point. By the Hartman-Grobman theorem, the flow of the nonlinear deterministic differential equations is topologically conjugate to the linear flow [17]. In Appendix B we derive a condition that identifies points on the stable manifolds of the linear and nonlinear system, respectively, by matching the timing of their asymptotic approach to the saddle point. Thus we determine the parameter δ from a matching condition of the flows of the original nonlinear system and of its linear approximation:

$$\delta = 2\left(\frac{2}{1+2\alpha}\right)^{\frac{2\alpha}{1-2\alpha}} \tag{18}$$

For our system with $\alpha = 0.1$ we find $\delta \approx 2.27$ and this indeed provides an excellent agreement for the distribution of passage times around one corner (*cf.* Fig. 5).

For weak noise, the mean single-quadrant first-passage times $\langle T_i \rangle$ may be written as a sum of a term depending logarithmically on the noise intensity, $\tau(D)$, and an $O(1)$ term, t_0 ([23], see also Eq. 35 below):

$$\langle T_i \rangle = \tau(D) + t_0, \qquad \text{as } D \to 0^+, \text{ for } i \in \{1, \ldots, 4\}, \tag{19}$$

where

$$\tau(D) = \lambda_u^{-1} \ln\left(\frac{\delta}{\sqrt{2D}}\right) \tag{20}$$

is the noise-dependent part of the mean transit time and the essential parameter in the following.

In the case of weak noise, we can make different approximations that vary in complexity. In the simplest approximation, we make two assumptions. First, we assume that $z_1(t)$ is well described by a dichotomous process

$$z_d(t) = 2[\Theta(z_1(t)) - 1/2], \tag{21}$$

where $\Theta(x)$ denotes the Heaviside jump function. For low noise, the variable $z_1(t)$ spends most of its time close to ± 1 and makes transitions on a fixed (approximately noise-

independent) time scale. Therefore, we assume the deviation between the two processes will be small, in the sense of

$$\langle (z_1(t) - z_d(t))^2 \rangle \ll \langle z_1^2(t) \rangle \tag{22}$$

(noting that the means of both processes vanish because of symmetry). We emphasize that although we neglect the continuous nature of the transition between the states, the transition time itself is included in the waiting times of the two states.

Second, we assume that the passage times through subsequent corners of the phase plane are statistically independent, which holds true in the vanishing-noise limit [1]. This assumption in turn entails that the residence times in the upstate/downstate are sums of two independent times, drawn from the same distribution, Eq. 16 and that all residence times in the two states are independent of each other. The probability density for this sum is given by the convolution of the density of the single corner-passage time with itself. The convolution condition implies that the Fourier transformation of the residence times satisfies $\tilde{\rho}_\pm(\omega) = \tilde{\rho}^2(\omega)$ (here $\tilde{\rho} = \int_0^\infty dt\, \rho(t) e^{i\omega t}$ with $\rho(t)$ from Eq. 16). Assuming independence of all residence times, we can apply the following formula for the power spectrum of an alternating renewal process with states $\eta_\pm$ and mean dwell times $\tau_\pm$ [24]

$$S_{\mathrm{d}}(\omega) = \frac{2(\eta_+ - \eta_-)^2}{(\tau_+ + \tau_-)\omega^2} \Re \left[\frac{(1 - \tilde{\rho}_+(\omega))(1 - \tilde{\rho}_-(\omega))}{1 - \tilde{\rho}_- \tilde{\rho}_+} \right] = \frac{2}{\langle T_i \rangle \omega^2} \Re \left[\frac{1 - \tilde{\rho}^2(\omega)}{1 + \tilde{\rho}^2(\omega)} \right]. \tag{23}$$

For our system $\eta_\pm = \pm 1$, $\tau_\pm = \langle T_1 + T_2 \rangle = \langle T_3 + T_4 \rangle$, and $\tilde{\rho}_\pm(\omega) = \tilde{\rho}^2(\omega)$ are the associated value, the mean residence time, and the Fourier transform of the residence time probability density of the state, respectively; for the simplification in the last step we have used the symmetries of the system and the aforementioned convolution relation for the residence times.

The preceding expression Eq. 23 gives the power spectrum in terms of the densities of the transit times through the successive quadrants (one for each saddle point) of the domain. We therefore investigate the form of these transition time densities and their dependence on D. For our approximation to hold, it is important that the formula Eq. 16 accurately describes the transit time density in our system. Fig. 5 compares Eq. 16 with numerical simulations, showing excellent agreement.

Fig. 5 suggests that $\rho_D(t)$ has the form of a stereotyped shape that merely translates as D decreases, at least for sufficiently small values of D. We wish to derive the form $\rho_D(t) = \rho(t - \tau(D))$. To this end, we first rewrite $\Delta_D(t)$ as follows, underlining terms referred to in the subsequent analysis

$$\Delta_D(t) = \left((\lambda_u^{-1} + \lambda_s^{-1}) e^{2\lambda_u (t - \tau(D))} - \underline{\lambda_u^{-1} e^{-2\lambda_u \tau(D)}} \right)^{-1/2}. \tag{24}$$

Here we have used $\delta = \sqrt{2D} e^{\lambda_u \tau}$, in accordance with Eqs. 17 and 20. Further, by straightforward algebraic manipulations we can rewrite the noise-dependent density $\rho_D(t)$ as

$$\rho_D(t) = \frac{2}{\sqrt{\pi}} \left(\lambda_u + \underline{\Delta_D^2(t) e^{-2\lambda_u \tau(D)}} \right) \Delta_D(t) e^{-\Delta_D^2(t)}. \tag{25}$$

Closer inspection reveals that for weak noise, $\rho_D(t)$ is appreciably greater than zero only for times close to $\tau(D)$. For such times, we may neglect the underlined terms in Eqs. 24 and 25, and obtain the approximations

$$\Delta_D(t) \approx \Delta(t - \tau(D)) \stackrel{!}{=} \frac{e^{-\lambda_u (t - \tau(D))}}{\sqrt{\lambda_u^{-1} + \lambda_s^{-1}}} \tag{26}$$

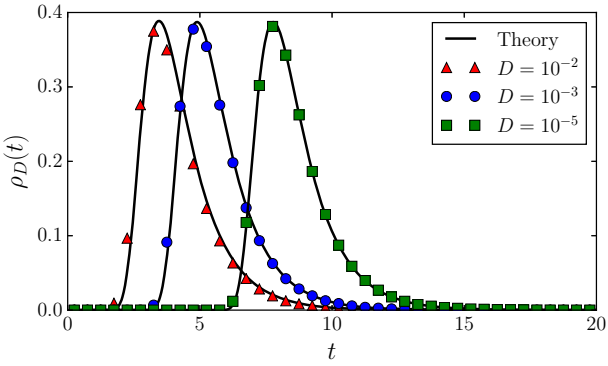

Fig. 5 Probability density of transit times T_i through a single quadrant of the system Eq. 1 for $\alpha = 0.1$ and different values of the noise intensity D, as indicated. Theoretical curves from Eq. 16 (*black lines*) are compared with simulation results (*symbols*), choosing the fitting parameter $\delta = 2.27$. Decreasing D causes a rightward shift in the density (increasing the mean transit time $\langle T_i \rangle$) while keeping its shape (including the width) constant

and

$$\rho_D(t) \approx \rho(t - \tau(D)) \stackrel{!}{=} \frac{2\lambda_u}{\sqrt{\pi}} \Delta e^{-\Delta^2}, \tag{27}$$

where $\Delta = \Delta(t - \tau(D))$ captures the D-dependence and reflects the rightward shift of ρ_D with decreasing noise. Moreover, both ρ_D and ρ are effectively zero for times less than $\tau(D)$ (minus a constant $O(1)$ offset), so we adopt $\rho(t)$ as an approximation to $\rho_D(t)$ over the entire range $t > 0$.

In order to calculate the power spectrum, the Fourier transform of $\rho(t)$ is needed; for this function we obtain

$$\tilde{\rho}(\omega) = \int_0^\infty dt\, e^{i\omega t} \rho(t - \tau(D)) = \int_{-\tau(D)}^\infty d\hat{t}\, e^{i\omega(\hat{t}+\tau(D))} \rho(\hat{t}) \approx e^{i\omega\tau(D)} \int_{-\infty}^\infty d\hat{t}\, e^{i\omega\hat{t}} \rho(\hat{t}) \tag{28}$$

The last approximation relies on the observation that $\rho(t) \to 0$ rapidly as t decreases below $\tau(D)$ and hence we can replace $-\tau(D)$ in the lower integration boundary by $-\infty$. Remarkably, the noise dependence of the Fourier transform is confined to the exponential prefactor.

The last integral in Eq. 28,

$$\tilde{\rho}_0(\omega) = \int_{-\infty}^\infty dt\, e^{i\omega t} \rho(t) \tag{29}$$

can be further simplified upon making the substitution

$$x = \frac{e^{-2\lambda_u t}}{\lambda_u^{-1} + \lambda_s^{-1}} \tag{30}$$

to the form

$$\tilde{\rho}_0(\omega) = \frac{\left(\lambda_u^{-1} + \lambda_s^{-1}\right)^{-i\omega/(2\lambda_u)}}{\sqrt{\pi}} \int_0^\infty dx\, x^{\left(-\frac{1}{2} - \frac{i\omega}{2\lambda_u}\right)} e^{-x}, \tag{31}$$

which reduces to a Gamma function with complex argument

$$\tilde{\rho}_0(\omega) = \frac{\Gamma\left(\frac{1}{2} - \frac{i\omega}{2\lambda_u}\right)}{\sqrt{\pi}\left(\lambda_u^{-1} + \lambda_s^{-1}\right)^{i\omega/(2\lambda_u)}}. \tag{32}$$

We thus obtain

$$\tilde{\rho}(\omega) = e^{i\omega\tau(D)} \frac{\Gamma\left(\frac{1}{2} - \frac{i\omega}{2\lambda_u}\right)}{\sqrt{\pi}\left(\lambda_u^{-1} + \lambda_s^{-1}\right)^{i\omega/(2\lambda_u)}} \tag{33}$$

The first derivative of $\tilde{\rho}_0$ at $\omega = 0$ gives us (together with $\tau(D)$) the mean single-quadrant transit time

$$\begin{aligned} \langle T_i \rangle &= \tau(D) + \frac{2\ln(2) + \gamma - \ln(\lambda_u^{-1} + \lambda_s^{-1})}{2\lambda_u} \\ &= \frac{-\ln(2D) + 2\ln(2\delta) + \gamma - \ln(\lambda_u^{-1} + \lambda_s^{-1})}{2\lambda_u} \end{aligned} \tag{34}$$

where $\gamma = 0.57721...$ is Euler's constant; hence, the second term in the first line is identical to the additive constant t_0 in Eq. 19:

$$t_0 = \frac{2\ln(2) + \gamma - \ln(\lambda_u^{-1} + \lambda_s^{-1})}{2\lambda_u}. \tag{35}$$

Differentiating $\tilde{\rho}_0$ a second time gives the second moment, from which we can determine the variance of the single-quadrant transit time as follows

$$\sigma_i^2 = \langle (T_i - \langle T_i \rangle)^2 \rangle = \frac{\pi^2}{8\lambda_u^2}. \tag{36}$$

This expression, remarkably, depends only on λ_u but neither on λ_s nor on the noise intensity D.

Substituting Eq. 32 into Eq. 23 yields the power spectrum for the discrete alternating process

$$S_{\mathrm{d}}(\omega) = \frac{2}{\omega^2(\tau(D) + t_0)} \Re\left(\frac{\pi(\lambda_u^{-1} + \lambda_s^{-1})^{i\omega/\lambda_u} - e^{2i\omega\tau(D)}\Gamma^2\left(\frac{1}{2} - \frac{i\omega}{2\lambda_u}\right)}{\pi(\lambda_u^{-1} + \lambda_s^{-1})^{i\omega/\lambda_u} + e^{2i\omega\tau(D)}\Gamma^2\left(\frac{1}{2} - \frac{i\omega}{2\lambda_u}\right)} \right). \tag{37}$$

The quality factor of an oscillation, Q, is the peak frequency, ω_{p}, divided by the full width at half maximum (FWHM), $\Delta\omega_p$. For low noise values the power spectrum is narrowly concentrated around the peak frequency $\omega_{\mathrm{p}} \approx \pi/(2\langle T_i \rangle)$. When the noise is small, the mean period is large, ω_{p} is small, and we can find an expression for the peak width by expanding $\tilde{\rho}(\omega)$ around $\omega = 0$. We translate the first passage time distribution by $\tau(D) + t_0$ to give a deviation with mean zero; the deviation has distribution ρ_{t_0}. With this notation, we may write the expansion

$$\tilde{\rho}(\omega) = e^{i\omega\tau(D)}\tilde{\rho}_0(\omega) = e^{i\omega(\tau(D)+t_0)}\tilde{\rho}_{t_0}(\omega) \tag{38}$$

$$\sim e^{i\omega(\tau(D)+t_0)}\left(1 - \frac{\omega^2\sigma_i^2}{2}\right) + O(\omega^3), \text{ as } |\omega| \to 0. \tag{39}$$

Expanding the power spectrum around $\omega = 0$ then gives the low-frequency dichotomous approximation to the power spectrum

$$S_{\mathrm{d,LF}}(\omega) = \frac{4\omega_{\mathrm{p}}}{\pi\omega^2}\,\Re\left(\frac{1 - e^{i\pi\omega/\omega_{\mathrm{p}}}\left(1 - \frac{\omega^2\sigma_i^2}{2}\right)^2}{1 + e^{i\pi\omega/\omega_{\mathrm{p}}}\left(1 - \frac{\omega^2\sigma_i^2}{2}\right)^2}\right). \tag{40}$$

where the approximate location of the peak is at

$$\omega_p = \frac{\pi/2}{\tau(D) + t_0}, \quad f_p = \frac{1}{4(\tau(D) + t_0)} \tag{41}$$

in cyclic and normal frequency, respectively. Therefore, for low noise, the height of the primary peak is given by

$$S_{\mathrm{p}} = S_{\mathrm{d,LF}}(\omega_{\mathrm{p}}) \approx \frac{8}{\pi\omega_{\mathrm{p}}^3\sigma^2} \tag{42}$$

while its width approaches

$$\Delta\omega_p \approx 2\sqrt{\frac{2}{S(\omega_{\mathrm{p}})\left.\frac{dS^{-1}(\omega)}{d\omega}\right|_{\omega=\omega_{\mathrm{p}}}}} \approx \frac{2\omega_p^3\sigma_i^2}{\pi}, \quad \Delta f_p \approx \frac{\omega_p^3\sigma_i^2}{\pi^2}. \tag{43}$$

where in both approximations we took into account only the leading orders in ω_p. Hence, in our simplest Lorentzian approximation, the spectrum around the primary peak reads

$$S_{\mathrm{d,Lorentz}} = \frac{8\omega_p^{-3}/(\pi\sigma^2)}{1 + \pi^2\sigma^{-4}\omega_p^{-6}(\omega - \omega_p)^2}. \tag{44}$$

The calculations above provide us also with an essential characteristics of noisy oscillations, the above mentioned quality factor, $Q = \omega_p/\Delta\omega_p$, given for our system in the limit of low noise by the simple expression

$$Q = \frac{\pi}{2\sigma_i^2}\omega_p^{-2}. \tag{45}$$

This means that we find a slow increase $Q \sim [\ln(1/D)]^2$ with decreasing noise intensity (for a comparison to simulation results, see below).

4.2 Smooth Approximation to the Full Process

The preceding approximations to the power spectrum based on a dichotomous process approximation ($S_{\mathrm{d}}(\omega)$, Eq. 37) and its expansion around low frequencies ($S_{\mathrm{d,LF}}(\omega)$, Eq. 42), neglected the smooth transitions between $z_1 \approx -1$ and $z_1 \approx +1$ in the full system given by Eq. 3. In this subsection we derive a correction to the discrete two-state process approximation. We require two assumptions to derive the form of the correction. First, the shape of the transitions from "down" to "up" (or vice versa) are stereotyped, and are not affected by the interval elapsed since the preceding transition. Second, as assumed previously, the transition times should be independent of the shape of the transition curve, and vice versa (the transition shape is independent of D, for small D).

In Fig. 6 we compare for a low noise level the dichotomous-process approximation and the original process $z_1(t)$ by plotting both the processes (top) and smoothed versions of

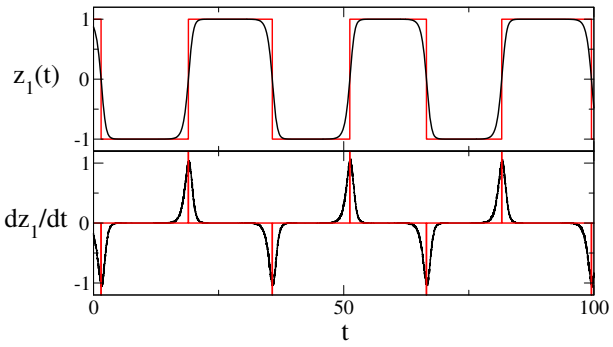

Fig. 6 A trace of the process and its dichotomous approximation (*top*) and the derivatives of the two processes (*bottom*) for $D = 10^{-5}$. The transition of the smooth process $z_1(t)$ becomes apparent by a stereotypic pulse in its derivative. Our theory for the power spectrum of $z_1(t)$ assumes that $\dot{z}_1(t) = g * \dot{z}_d(t)$, where the star denotes convolution with the pulse shape $g(t)$, to be determined from the dynamics of the deterministic system

their temporal derivative (bottom). It becomes clear that the smooth transition in the original process is mainly characterized by a stereotypic pulse shape $2g(t)$ in the process' temporal derivative. This suggests to approximate

$$\dot{z}_1(t) = g * \dot{z}_d(t) \tag{46}$$

by a convolution of the derivative of the dichotomous process (which is an alternating sequence of delta spikes) with this pulse shape. Note that we do not take into account the white-noise fluctuations that are part of $\dot{z}_1(t)$ according to its Langevin equation Eq. 3.

Once we have found $g(t)$ and its Fourier transform $\tilde{g}(\omega)$, the power spectrum of the continuous process can be approximated by

$$S_{\text{cont}}(\omega) = |\tilde{g}(\omega)|^2 S_{\text{d}}(\omega). \tag{47}$$

The profile $g(t)$ and its Fourier transform can be found from an analysis of the deterministic system. We first note that in order to describe the deterministic transition between ± 1, it is justified to set $z_2(t) = 1$ because during the transition of $z_1(t)$ the value of the other variable is indeed very close to 1 and the small discrepancy does not affect the time course of $z_1(t)$ much. Neglecting thus both the variations in $z_2(t)$ and the noise $\xi_1(t)$, the dynamics of the transition is governed by

$$\dot{z}_1 = (1 - z_1^2)(2\alpha z_1 + 1), \tag{48}$$

which can be solved implicitly

$$t(z_1) = \int^{z_1} \frac{dz}{(1-z^2)(2\alpha z + 1)} = \frac{\ln(z_1+1)}{2-4\alpha} - \frac{\ln(1-z_1)}{2+4\alpha} - \frac{2\alpha \ln(1+2\alpha z_1)}{(1-4\alpha^2)}. \tag{49}$$

Furthermore, we know the derivative as a function of z_1, namely $\dot{z}_1(z_1)$ given by the right-hand side of Eq. 48. Hence, we can parametrically plot both the time t and the profile $g(t)$ as functions of z_1, i.e. $[t(z_1), 2g(t) = \dot{z}_1(z_1)]$, where z_1 varies between ± 1. This is compared in Fig. 7a to a smoothed version of the temporal derivative and shows very good agreement (also on a logarithmic scale, displayed in the inset).

What we need in the expression for the power spectrum though is the Fourier transform of the transition profile. This can be simplified by changing in the Fourier transform from time integration to an integration over z_1 as follows

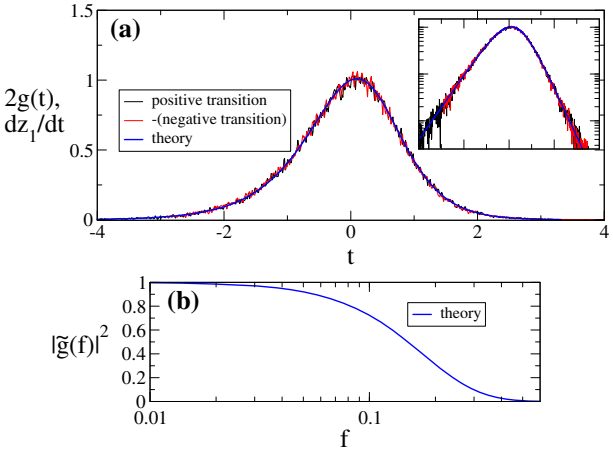

Fig. 7 The derivative of the transition function (**a**) and its Fourier transform (**b**). In (**a**) we show two of the pulses from Fig. 6 *bottom* a positive (upward) pulse and a (here inverted) downward pulse demonstrating the symmetry between upward and downward transitions. Superimposed is the theory, Eqs. 49 and 48. In (**b**) the Fourier transform according to the analytical solution, Eq. 51, is shown

$$\tilde{g}(\omega) = \frac{1}{2}\int_{-\infty}^{\infty} dt\ \dot{z}_1(t)\exp[i\omega t] = \frac{1}{2}\int_{-1}^{1} dz\ \exp[i\omega t(z)]. \tag{50}$$

This integral can either be evaluated numerically or expressed by a higher mathematical function, the hypergeometric function F_1 (Appell's Hypergeometric function of the first kind):

$$\tilde{g}(\omega) = -\frac{2^{1+\frac{i\omega}{2-4\alpha}}(1-z)^{1-\frac{i\omega}{2+4\alpha}}(1+2\alpha)^{1-\frac{2i\alpha\omega}{1-4\alpha^2}}}{(2+4\alpha-i\omega)} \times F_1\left(1-\frac{i\omega}{2+4\alpha}, \frac{i\omega}{-2+4\alpha}, \frac{2i\alpha\omega}{1-4\alpha^2}, 2-\frac{i\omega}{2+4\alpha}, \frac{1-z}{2}, \frac{2\alpha(1-z)}{1+2\alpha}\right). \tag{51}$$

The filter function is shown in Fig. 7b and displays a strictly monotonic decrease. As we tacitly used in our previous pure two-state theory, the smooth transition has little effect on very small frequencies, where the function is constant. It will be shown below that $g(\omega)$ determines in particular the behavior of the power spectrum at intermediate frequencies.

4.3 Comparison of the Different Approximations to Numerical Simulations

In order to get an impression of how reliable the different approximations are, we compare in Fig. 8 the spectra obtained from numerical simulations of Eq. 1 to the various expressions.

In Fig. 8a, b we show simulation data for a comparatively large noise intensity of $D = 10^{-2}$ (filled circles). At this noise level, the Lorentzian spectrum, Eq. 44, gives a reasonable approximation to the primary peak but also displays some deviations in peak height. This is also the case for the other approximations (not shown). In Fig. 8b we show the spectrum on a semi-logarithmic scale, revealing the behavior in the high-frequency range. At this noise level both the full and the low-frequency approximations capture the shape of the primary peak but fail to reproduce accurately the shoulder and the fall-off at higher frequencies. The latter are

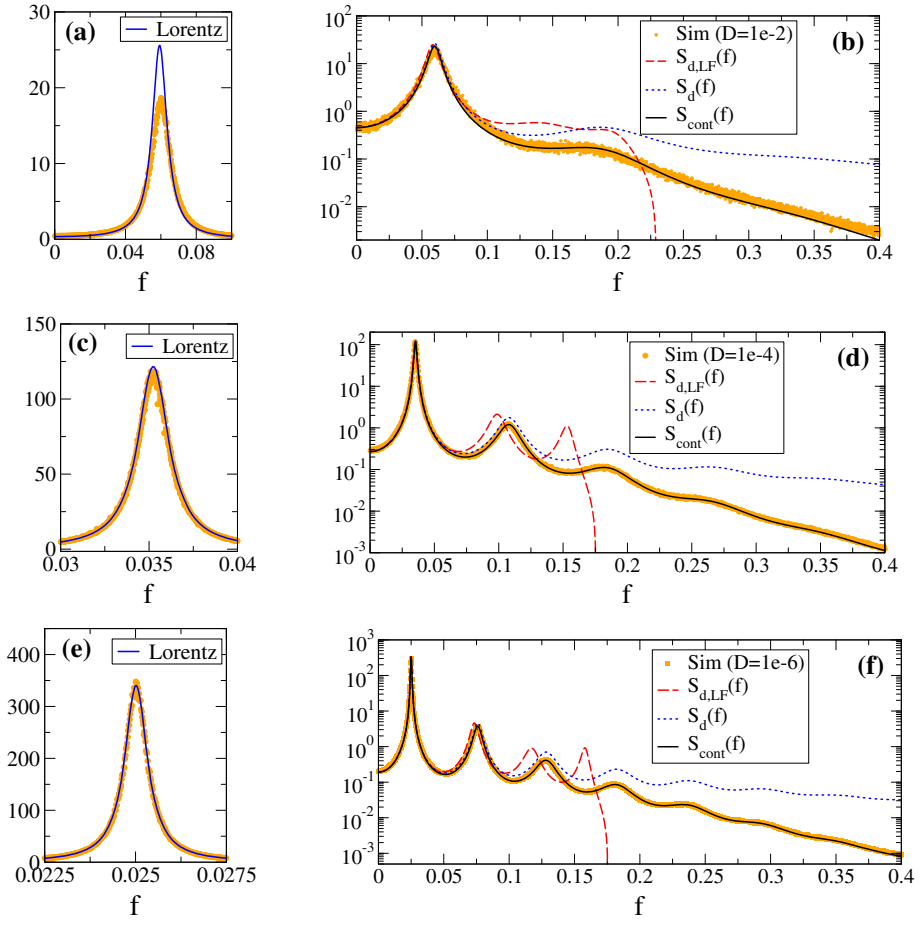

Fig. 8 Power spectra for different noise intensities as indicated. Simulation results of the Langevin Eq. 1 are compared on linear axes to the Lorentzian approximation, Eq. 44, *on the left* (**a**, **c**, **e**); *on the right* (**b**, **d**, **f**), comparison in a semi-logarithmic presentation to the more involved approximations (*lines*): dichotomous-process approximation, Eq. 37 (*blue dotted*), low-frequency approximation Eq. 40 (*dashed red*), and continuous-process approximation, Eq. 47 (*solid black*)

caused by the smooth transition between the states as proven by the excellent improvement with the continuous approximation, Eq. 47.

With decreasing noise intensity ($D = 10^{-4}$ in Fig. 8c, d), we see a better agreement of all approximations in their respective range of validity: the simple Lorentzian formula (Fig. 8c) gives an excellent approximation at the linear scale, including the position and width of the peak. The full dichotomous expression provides an excellent agreement over the entire primary peak, and the continuous solution reproduces the entire curve including the two higher harmonics and the overall decrease with frequencies at higher f. All these observations can be also made for a further decreased noise level of $D = 10^{-6}$ shown in (Fig. 8e, f), except that this lower noise intensity leads to even more higher harmonics than before.

We also have to mention that our analytical result for the power spectrum does not include an extremely weak contribution that emerges in the high-frequency limit, i.e. beyond the

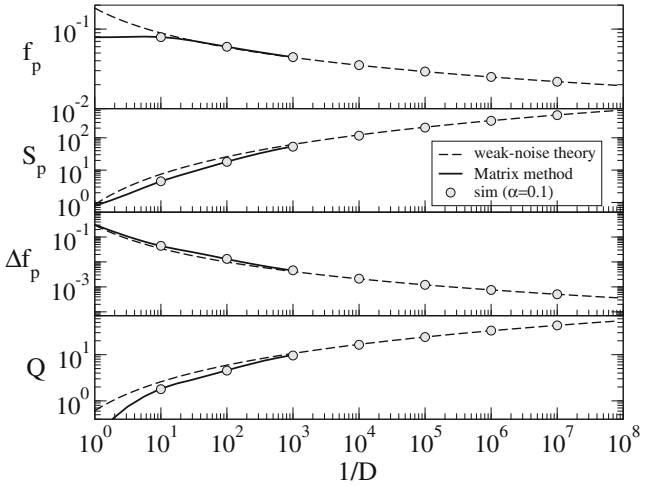

Fig. 9 Characteristics of the oscillation—theory (*lines*) against simulation results (*symbols*) for $\alpha = 0.1$. From *top to bottom* frequency of oscillation, Eq. 41, peak height, Eq. 42, full width at half maximum, Eq. 43, and quality factor, Eq. 45. Simulation results for the parameters were determined by fitting Lorentz functions to spectra such as that in Fig. 8a

frequency range shown in Fig. 8. According to Eq. 3, the derivative $\dot{z}_1$ does not only possess the smooth transition function that we have discussed above but has also a component that is directly proportional to the driving multiplicative white noise, $\sqrt{2D[1 - z_1^2(t)]}\xi_1(t)$.

Finally, we compare our theoretical results for the characteristics of the primary peak to numerical simulations in Fig. 9 as functions of the inverse noise intensity. The results of the matrix-inversion method (solid lines) display excellent agreement with the numerical simulation at larger noise intensities (left side of the plot) but is restricted to moderate to large noise. Fortunately, at the point where the matrix method stops working, the weak-noise results (dashed lines) are already close to them. Moreover, the weak-noise formulas are confirmed by simulation results performed at even smaller noise intensities ($D \leq 10^{-3}$).

Generally, it is remarkable how slowly the statistics changes with a decrease of the noise intensity. The quality factor, for instance, changes by a little more than one order of magnitude if we decrease the noise intensity by six orders of magnitude. The frequency does not even change by one order of magnitude in the same range of noise intensities. This illustrates that in a dynamical system with heteroclinic orbits already tiny amounts of noise can cause robust stochastic oscillations with intermediate time scales and considerable variability.

5 Summary and Conclusions

In this paper we have studied the noise dependence of the power spectrum of a heteroclinic stochastic oscillator. We used different analytical and semi-analytical methods to characterize the spectrum.

For stable limit cycle systems that oscillate in the absence of noise, the effects of small noise perturbations may be studied in a simple manner *via* reduction to a one-dimensional phase variable [4]. For excitable systems, sustained oscillations vanish in the small noise limit [12]. Stable heteroclinic systems [16,18–20] exist, in a sense, on the boundary between these

two scenarios. Without noise, an autonomous heteroclinic system does not show sustained finite period oscillation. But with increasing noise, we expect oscillations to deteriorate. It is therefore of interest to ask how the character of the oscillations behaves as their source—the amplitude of noise forcing—is reduced to vanishing levels. We resolved this question here through analysis of the power spectrum, in particular the quality factor of the principal peak, for which we find a slow but steady increase as noise intensity decreases.

In the first part we introduced a numerical scheme that is based on the Fokker–Planck equation and gives us full access to the entire power spectrum if the noise is not too weak. It is simple to understand the latter limitation: our solution involves the steady-state probability density and other functions of the state-space variables that become strongly peaked in the limit of weak noise. Because the scheme is based on an expansion into trigonometric functions, it is evident that extremely peaked functions will require a large number of terms in the respective expansion, making the involved matrix manipulations infeasible at some point.

Fortunately, it turns out that the system is analytically tractable to a large extent exactly in the weak-noise limit, in which the Fokker–Planck method fails. We developed a number of approximations to derive more and more accurate descriptions of the power spectrum. First, we approximated the dominant temporal variation in the observable $z_1(t)$ as a dichotomous noise, i.e. a symmetric alternating renewal process. Using the first-transit-time results for a passage along a saddle point by Stones and Holmes [23] and simplifying these results in particular in the Fourier domain we derived an accurate description of the primary peak of the power spectrum, including simple formulas for the peak frequency, the peak width and the quality factor.

We could furthermore extend an improved formula for the power spectrum valid for higher frequencies by taking into account the smoothness of the transitions between the states. This led to a low-pass filter function by which the spectrum of the dichotomous process has to be multiplied. The comparison with numerical simulations revealed a good agreement of this full spectrum from low to intermediate frequencies for a range that accounts for almost all of the variance of the process.

The simple formulas for the peak frequency and quality factor of the primary peak illustrated a rather weak dependence of the heteroclinic system on the noise intensity. The quality factor essentially increases as $\left[\ln(D^{-1})\right]^2$ as the noise intensity is decreased. This implies that already tiny perturbations can lead to pronounced stochastic oscillations, which is certainly related to the fact that we are exactly at a bifurcation point. The heteroclinic connections between successive saddles are not structurally stable, and can be broken by a static perturbation such as adding a twist to the vector field. For instance, writing the system Eq. 1 as $\dot{y}_1 = f_1(y_1, y_2) + \sqrt{2D}\xi_1(t)$ and $\dot{y}_2 = f_2(y_1, y_2) + \sqrt{2D}\xi_2(t)$, the perturbed system

$$\begin{aligned} \dot{y}_1 &= f_1(y_1, y_2) + \mu f_2(y_1, y_2) + \sqrt{2D}\xi_1(t), \\ \dot{y}_2 &= f_2(y_1, y_2) - \mu f_1(y_1, y_2) + \sqrt{2D}\xi_2(t) \end{aligned} \tag{52}$$

when $D = 0$ and $1 \gg \mu > 0$ has a stable limit cycle in the domain $-\pi/2 < \{y_1, y_2\} < \pi/2$. As shown in [22], the deterministic system's infinitesimal phase response curve (iPRC) exhibits extreme sensitivity to perturbations at specific phases of the limit cycle, when $\mu > 0$ is small, consistent with our observation here of a large impact arising from small stochastic perturbations. However, as μ is increased, we expect a smoothened dependence on the noise.

The methods that we have used in this paper may be also employed for the study of power spectra of other systems with heteroclinic cycles. If a projection of a variable on a two-state process is sufficient, we can use the same alternating renewal formula but have to modify the

residence time probability densities in the respective states accordingly. If a small number of states is involved (but more than two), the formulas for the two-state process [24] may be generalizable. More difficult appear extensions to cases, in which the noise acts only on one of the dynamical variables or in which fluctuations are correlated in time or have non-Gaussian statistics. We hope, nonetheless, that the example system studied in our paper may give some guidance in the study of power spectra in more complicated systems.

Acknowledgements JGB, PJT, and BL would like to acknowledge funding by La Caixa and DAAD (program 50015239), the National Science Foundation (Grant DMS-1413770), and BMBF (FKZ: 486 01GQ1001A) respectively.

Appendix A: Details on the Numerical Determination of the Spectrum from the Fokker–Planck Equation (Matrix-Inversion Method)

In Sect. 3 we derived two partial differential equations that determine the power spectrum. Here we show how these equations can be solved numerically by an eigenfunction expansion (for further details, see [6]).

Expansion into a Complete set of Functions

The power spectrum $S_{zz}(\omega)$ is given in Eq. 9 in terms of an auxiliary function $\tilde{H}(\mathbf{y};\omega)$, which is defined in Eq. 10 and satisfies the two-dimensional, second-order, partial differential equations,

$$\mathcal{L}_{\mathrm{FP}}(\mathbf{y})P_0(\mathbf{y}) = 0, \tag{7 revisited}$$

$$\left(\mathcal{L}_{\mathrm{FP}}(\mathbf{y}) + i\omega\mathcal{I}\right)\tilde{H}(\mathbf{y};\omega) = -P_0(\mathbf{y})\left[f(\mathbf{y}) - \langle f(\mathbf{y})\rangle\right], \tag{11 revisited}$$

where $P_0(\mathbf{y})$ is the stationary probability distribution and $\mathcal{L}_{\mathrm{FP}}$ is the Fokker–Planck operator associated to $\mathbf{y}(t)$. The solution to this system of partial differential equations may be found by expanding $P_0(\mathbf{y})$ and $\tilde{H}(\mathbf{y};\omega)$ into an appropriate basis of functions that satisfy the boundary conditions.

The heteroclinic oscillator system Eq. 1 with reflecting boundary conditions on the domain $\Omega = [-\pi/2, \pi/2] \times [-\pi/2, \pi/2]$ can be shown to be equivalent (for certain observables $f(\mathbf{y})$, such as $z_i = \sin(y_i)$) to a system with periodic boundary conditions on $\Omega' = [-\pi, \pi] \times [-\pi, \pi]$ and the same dynamics. Thus, we expand the solutions into the basis of harmonic functions with period $L_i = 2\pi$ in both y_1 and y_2, i.e.

$$P_0(\mathbf{y}) = \sum_{m=-\infty}^{\infty}\sum_{l=-\infty}^{\infty} c_{m,l}e^{i(k_1 m y_1 + k_2 l y_2)} = \sum_{m=-\infty}^{\infty}\sum_{l=-\infty}^{\infty} c_{m,l}e^{i(m y_1 + l y_2)}. \tag{12 revisited}$$

and, similarly,

$$\tilde{H}(\mathbf{y};\omega) = \sum_{m=-\infty}^{\infty}\sum_{l=-\infty}^{\infty} \tilde{H}_{m,l}(\omega)e^{i(m y_1 + l y_2)}. \tag{13 revisited}$$

Inserting Eq. 12 into Eq. 7, grouping the terms associated to each basis function $e^{imy_1}e^{ily_2}$, and requiring that these terms should vanish for every combination m, l, we obtain for the coefficients of the steady state distribution

$$0 = -\tfrac{1}{4}\Big[(m-l)c_{m-1,l-1} + (m+l)c_{m+1,l-1} - (m-l)c_{m+1,l+1}$$

Table 1 Summary of the conditions imposed by symmetries (other than 2π-periodicity on y_1 and y_2) on the auxiliary function $\tilde{H}(\mathbf{y};\omega)$ and its expansion coefficients $\tilde{H}(\omega)$

Symmetry transformation	$\tilde{H}(\mathbf{y};\omega)$	$\tilde{H}_{m,l}(\omega)$
$\mathbf{y} \mapsto -\mathbf{y}$	$\tilde{H}(\mathbf{y};\omega) = -\tilde{H}(-\mathbf{y};\omega)$	$\tilde{H}_{-m,-l} = -\tilde{H}_{m,l}$
$(y_1, y_2) \mapsto (y_1 + k\pi, y_2 \pm k\pi)$, $k \in \mathbb{Z}$	$\tilde{H}(y_1 + k\pi, y_2 \pm k\pi;\omega) = -\tilde{H}(y_1, y_2;\omega)$	$\tilde{H}_{m,l} = 0$, if $m + l = 2k$

$$-(m+l)c_{m-1,l+1} + 2\alpha m c_{m-2,l} + 2\alpha l c_{m,l-2}$$
$$-2\alpha m c_{m+2,l} - 2\alpha l c_{m,l+2} + 4D(m^2+l^2)c_{m,l}\Big], \quad \forall m, l \in \mathbb{Z}. \tag{A1}$$

Additional symmetries present in the system impose further constraints on the set of coefficients $\{c_{m,l}\}$: (i) because $\mathcal{L}_{\mathrm{FP}}(-\mathbf{y}) = \mathcal{L}_{\mathrm{FP}}(\mathbf{y})$ the density is symmetric under inversion, $P_0(-\mathbf{y}) = P_0(\mathbf{y})$, from which we find $c_{-m,-l} = c_{m,l}$; (ii) $\mathcal{L}_{\mathrm{FP}}(\mathbf{y})$ is also invariant under the translations $(y_1, y_2) \mapsto (y_1 + 2\pi k, y_2)$ and $(y_1, y_2) \mapsto (y_1, y_2 + 2\pi k)$, from which we can infer that $c_{m,l} = 0$ if $m+l = 2k+1$, $k \in \mathbb{Z}$; (iii) because $P_0(\mathbf{y})$ is real-valued, $c_{-m,-l} = c^*_{m,l}$. Finally, from the normalization condition follows $c_{0,0} = \pi^{-2}$.

If we insert the expansions Eqs. 13 and 12 into Eq. 11 with $f(y_1) = \sin(y_1)$ and follow the derivation for $P_0(\mathbf{y})$ above, we obtain

$$\begin{aligned}
&-\frac{1}{4}\Big[(m-l)\tilde{H}_{m-1,l-1} + (m+l)\tilde{H}_{m+1,l-1} - (m-l)\tilde{H}_{m+1,l+1} - (m+l)\tilde{H}_{m-1,l+1} \\
&\quad + 2\alpha l\tilde{H}_{m,l-2} + 2\alpha m\tilde{H}_{m-2,l} - 2\alpha m\tilde{H}_{m+2,l} - 2\alpha l\tilde{H}_{m,l+2} \\
&\quad + \left(4D(m^2+l^2) - 4i\omega\right)\tilde{H}_{m,l}\Big] \\
&= \frac{1}{2i}\left[(2\pi)^2 c_{m,l}(c_{1,0} - c_{-1,0}) - (c_{m-1,l} - c_{m+1,l})\right], \quad \forall m, l \in \mathbb{Z}.
\end{aligned} \tag{A2}$$

This defines an infinite *inhomogeneous* system of linear equations. From the underlying symmetries of the problem follow further conditions on the coefficients (see Table 1).

Finally, to obtain the power spectrum $S_{zz}(\omega)$ in terms of the coefficients, we plug Eq. 13 into Eq. 9 and use the orthogonality relations for the Fourier basis:

$$S_{xx}(\omega) = 2(2\pi)\Re\left[\sum_m \tilde{H}_{m,0}\int dy_1 f(y_1)e^{imy_1}\right].$$

Choosing our observable to be $z = f(y_1) = \sin(y_1) = (e^{iy_1} - e^{-iy_1})/(2i)$ and using $\tilde{H}_{m,l} = -\tilde{H}_{-m,-l}$ leads to

$$S_{xx}(\omega) = 2(2\pi)^2\Re\Big[i\tilde{H}_{0,1}(\omega)\Big] = -8\pi^2\Im\Big[\tilde{H}_{0,1}(\omega)\Big], \tag{14 revisited}$$

where $\Im[\cdot]$ denotes the imaginary part of the argument.

Solving the Full Linear System

We start by solving the system Eq. A2 for the coefficients $c_{m,l}$ of the expansion of $P_0(\mathbf{y})$; this allows us to construct Eq. A2, which is then solved for the coefficients $\tilde{H}_{m,l}(\omega)$ of the expansion of $\tilde{H}(\mathbf{y};\omega)$ at each ω. From there, the power spectrum Eq. 14 is evaluated.

In the first place, we truncate the set of basis functions $\{e^{imy_1}e^{ily_2}\}$, $-L \leq m, l \leq L$ and choose a specific ordering of its elements, according to which the coefficients $c_{m,l}$ (resp. $\tilde{H}_{m,l}(\omega)$) are arranged into a column vector $\mathbf{c}$ (resp. $\mathbf{h}_\omega$) which looks as follows

$$\mathbf{c}^{(L)} = \left[c_{-L,-L}, \ldots, c_{-L,L}, \cdots, c_{0,-L}, \ldots, c_{0,L}, \ldots, c_{L,-L}, \cdots, c_{L,L}\right]^T,$$

where ^{T} denotes transposition and $\mathbf{c}^{(L)}$ indicates that the size of $\mathbf{c}$ depends on the truncation parameter L. Note that each entry of $\mathbf{c}^{(L)}$ corresponds to a coefficient $c_{m,l}$ associated to a basis function $e^{imy_1}e^{ily_2}$, i.e.

$$\left[\mathbf{c}^{(L)}\right]_{m(2L+1)+l} = c_{m,l}, \quad -L \leq m, l \leq L.$$

One can define $\mathbf{h}_\omega$ analogously. The chosen ordering is also used to set the elements of the matrices $\mathbf{M}$ and $\mathbf{A}_\omega$ of coefficients of the linear systems Eqs. A1 and A2, as well as the inhomogeneity $\mathbf{f}$ on the RHS of Eq. A2.

With the previous ingredients we can write the equivalent of Eqs. 7 and 11 in matrix form as

$$\mathbf{M}^{(L)}(D, \alpha)\mathbf{c}^{(L)} = 0, \tag{A3}$$

$$\mathbf{A}_\omega^{(L)}(D, \alpha; \omega)\mathbf{h}_\omega^{(L)} = \mathbf{f}^{(L)}, \tag{A4}$$

where we have indicated the dependences of $\mathbf{M}$ and $\mathbf{A}_\omega$ on the noise intensity D, the stability parameter α and the frequency at which we evaluate the power spectrum ω. After solving Eq. A3 once, we can determine $\mathbf{f}$ and solve Eq. A4 for $\mathbf{h}_\omega$ at a set of discrete frequencies $\{\omega_i\}, i \in 1, \ldots, N$ to evaluate the power spectrum $S(\omega)$ in a given frequency window.

The applicability of the numerical method outlined above is limited by the size of the matrices $\mathbf{M}^{(L)}$ and $\mathbf{A}_\omega^{(L)}$, which is determined by the truncation parameter L. In particular, the dimension of $\mathbf{M}^{(L)}$ and $\mathbf{A}_\omega^{(L)}$ grows as $(2L+1)^2 \times (2L+1)^2$, thus even small values of L yield large matrices. Solving linear systems described by large matrices is memory- and CPU-demanding. However, the use of efficient sparse matrix methods ($\mathbf{M}^{(L)}$ and $\mathbf{A}_\omega^{(L)}$ have very few non-zero entries) may alleviate these problems.

The issue of the high-dimensionality of the system becomes manifest prominently in the low-noise regime, which feature probability distributions displaying very abrupt changes on small spatial scales. In such cases, one must increase L in order to include modes $e^{imy_1}e^{ily_2}$ with higher spatial frequencies $|\mathbf{k}| = \sqrt{m^2 + l^2}$ in the expansion of $P_0(\mathbf{y})$ and $\tilde{H}(\mathbf{y}; \omega)$. This will limit in practice the applicability of the matrix-inversion method in the weak-noise regime, even if using sparse methods.

Appendix B: Estimating the Parameter $\delta(\alpha)$

Here we show how to calculate the value of δ from a matching condition.

For our original system Eq. 1 in the absence of noise, i.e. for

$$\begin{aligned} \dot{y}_1 &= \cos(y_1)\sin(y_2) + \alpha \sin(2y_1), \\ \dot{y}_2 &= -\sin(y_1)\cos(y_2) + \alpha \sin(2y_2) \end{aligned} \tag{B1}$$

the eigenvalues at the saddle points are $\pm 1 - 2\alpha$, and the saddles are located at $(\pm\pi/2, \pm\pi/2)$. Consider the saddle located at $(\pi/2, \pi/2)$. The quadrant surrounding this point is the region bordered by the ingress boundary ($y_1 = 0, 0 < y_2 \leq \pi/2$) and the egress boundary ($0 < y_1 \leq \pi/2, y_2 = 0$) (cf. Fig. 10). At this saddle, the stable eigenvector is $(1, 0)$ and the

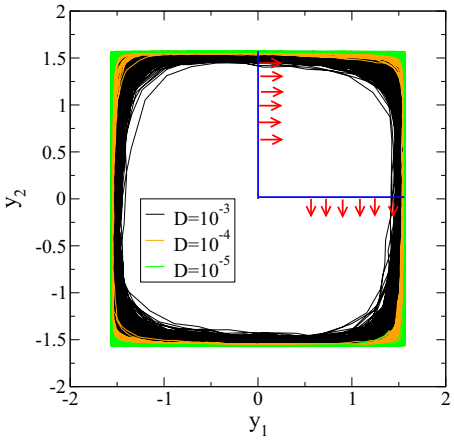

Fig. 10 For illustration, we show simulated trajectories for different noise intensities as indicated. Referring to the saddle point at $(\pi/2, \pi/2)$, the *vertical* and *horizontal blue lines* indicate the ingress and egress boundaries, respectively

unstable one is (0, 1). The difficulty in estimating the effective value of δ is that the flow in this square is nonlinear.

Consider the deterministic linearization of the flow around the saddle at $(\pi/2, \pi/2)$ in terms of the variables u_1 and u_2:

$$\dot{u}_1 = (-1 - 2\alpha)u_1 \tag{B2}$$

$$\dot{u}_2 = (1 - 2\alpha)u_2. \tag{B3}$$

We are interested in matching the properties (namely the first passage time distribution) of the linearized and nonlinear systems when the noise is very small. Thus, we aim to establish an explicit mapping between the deterministic flow of the linearized system and the deterministic flow of the nonlinear system, because for small noise the effect on the trajectories only comes into play close to the fixed point, where the linearization is accurate.

For the linearized system the ingress boundary is given by $u_1 = \delta, 0 \leq u_2 < \delta$. In order to determine δ we use the matching properties of the flows. In particular, we consider the flow along an invariant subset, namely the solution

$$u_1(t) = \delta e^{(-1-2\alpha)t}, \quad u_2(t) = 0 \tag{B4}$$

which corresponds to the solution of the initial value problem starting from the ingress boundary

$$y_1(0) = 0, \quad y_2(0) = \pi/2. \tag{B5}$$

Thus we wish to solve the initial value problem

$$\dot{y} = \cos(y) + \alpha \sin(2y), \quad y(0) = 0, \tag{B6}$$

and choose δ so that the linearized flow matches as the trajectories approach the saddle point. That is, we wish to choose δ so that

$$\lim_{t\to\infty} \frac{\frac{\pi}{2} - y(t)}{\delta e^{(-1-2\alpha)t}} = 1. \tag{B7}$$

Or, equivalently, we set

$$\delta = \lim_{t\to\infty} \left[e^{(1+2\alpha)t} \left(\frac{\pi}{2} - y(t) \right) \right]. \tag{B8}$$

We can simplify this as follows: We use the relation $y_1(t) = \arcsin(z_1(t))$ and the implicit solution for $z_1(t)$, Eq. 49 in the asymptotic limit $t \to \infty$. In this limit, z_1 is very close to 1 and the time variable $t(z_1)$ is dominated by the logarithm $\ln(1 - z_1)$. For a more precise approximation of Eq. 49 in the asymptotic limit, we can set $z_1 = 1$ in the other two logarithmic terms

$$t(z_1) = \frac{\ln(2)}{2 - 4\alpha} - \frac{2\alpha \ln(1 + 2\alpha)}{1 - 4\alpha^2} - \frac{\ln(1 - z_1)}{2 + 4\alpha} = t_s - \frac{\ln(1 - z_1)}{2 + 4\alpha}, \tag{B9}$$

where t_s is the constant defined by the first two terms. This equation can be quickly solved for z_1:

$$z_1(t) = 1 - \exp\left[-(2 + 4\alpha)(t - t_s)\right], \qquad t \to \infty \tag{B10}$$

Making use of the series expansion

$$\arcsin(1 - \varepsilon) \approx \frac{\pi}{2} - \sqrt{2\varepsilon}, \qquad \varepsilon \ll 1 \tag{B11}$$

we find exactly the inverse of the diverging prefactor and the finite limit for δ:

$$\delta = \lim_{t \to \infty} e^{(1+2\alpha)t} \sqrt{2} e^{-(1+2\alpha)(t - t_s)} = \sqrt{2} \exp\left[(1 + 2\alpha) t_s\right], \tag{B12}$$

which can be further simplified by Eq. B9, yielding Eq. 18.

References

1. Bakhtin, Y.: Noisy heteroclinic networks. Probab. Theory Relat. Fields **150**(1–2), 1 (2011)
2. Burns, S., Xing, D., Shapley, R.: Is gamma-band activity in the local field potential of V1 cortex a "clock" or filtered noise? J. Neurosci. **31**, 9658 (2011)
3. Elowitz, M.B., Leibler, S.: A synthetic oscillatory network of transcriptional regulators. Nature **403**, 335 (2000)
4. Ermentrout, G.B., Beverlin, B., Troyer, T., Netoff, T.I.: The variance of phase-resetting curves. J. Comput. Neurosci. **31**(2), 185–197 (2011)
5. Gardiner, C.W.: Handbook of Stochastic Methods. Springer, Berlin (1985)
6. Giner-Baldó, J.: Stochastic oscillations and their power spectrum. Master's thesis, Freie Universität Berlin (2016)
7. Gleeson, J.P., O'Doherty, F.: Non-Lorentzian spectral lineshapes near a Hopf bifurcation. SIAM J. Appl. Math. **66**(5), 1669–1688 (2006)
8. Hirsch, M.W., Smale, S., Devaney, R.L.: Differential Equations, Dynamical Systems, and an Introduction to Chaos. Academic Press, Amsterdam (2012)
9. Jülicher, F., Dierkes, K., Lindner, B., Prost, J., Martin, P.: Spontaneous movements and linear response of a noisy oscillator. Eur. Phys. J. E. **29**(4), 449 (2009)
10. Jung, P.: Periodically driven stochastic systems. Phys. Rep. **234**, 175 (1993)
11. Kummer, U., Krajnc, B., Pahle, J., Green, A.K., Dixon, C.J., Marhl, M.: Transition from stochastic to deterministic behavior in calcium oscillations. Biophys. J. **89**, 1603 (2005)
12. Lindner, B., García-Ojalvo, J., Neiman, A., Schimansky-Geier, L.: Effects of noise in excitable systems. Phys. Rep. **392**(6), 321–424 (2004)
13. Lindner, B., Schimansky-Geier, L.: Coherence and stochastic resonance in a two-state system. Phys. Rev. E. **61**, 6103 (2000)
14. Lindner, B., Sokolov, I.M.: Giant diffusion of underdamped particles in a biased periodic potential. Phys. Rev. E **93**, 042106 (2016)
15. Martin, P., Bozovic, D., Choe, Y., Hudspeth, A.J.: Spontaneous oscillation by hair bundles of the bullfrog's sacculus. J. Neurosci. **23**, 4533 (2003)
16. May, R.M., Leonard, W.J.: Nonlinear aspects of competition between three species. SIAM J. Appl. Math. **29**(2), 243–253 (1975)
17. Meiss, J.D.: Differential Dynamical Systems. Society for Industrial and Applied Mathematics, Philadelphia (2007)
18. Rabinovich, M.I., Huerta, R., Varona, P., Afraimovich, V.S.: Transient cognitive dynamics, metastability, and decision making. PLoS Comput. Biol. **4**(5), e1000072 (2008)

19. Rabinovich, M.I., Lecanda, P., Huerta, R., Abarbanel, H.D.I., Laurent, G.: Dynamical encoding by networks of competing neuron groups: winnerless competition. Phys. Rev. Lett. **87**(6), 068102 (2001)
20. Rabinovich, M.I., Selverston, A.I., Abarbanel, H.D.I.: Dynamical principles in neuroscience. Rev. Mod. Phys. **78**, 1213 (2006)
21. Risken, H.: The Fokker-Planck Equation. Springer, Berlin (1984)
22. Shaw, K.M., Park, Y.-M., Chiel, H.J., Thomas, P.J.: Phase resetting in an asymptotically phaseless system: on the phase response of limit cycles verging on a heteroclinic orbit. SIAM J. Appl. Dyn. Syst. **11**(1), 350 (2012)
23. Stone, E., Holmes, P.: Random perturbations of heteroclinic attractors. SIAM J. Appl. Math. **50**, 726 (1990)
24. Stratonovich, R.L.: Topics in the Theory of Random Noise. Gordon and Breach, New York (1967)
25. Thomas, P.J., Lindner, B.: Asymptotic phase of stochastic oscillators. Phys. Rev. Lett. **113**, 254101 (2014)